Supporting Information

How does local strain affect Stokes shifts in halide double perovskite nanocrystals?

Saar Shaek[1,2], Sasha Khalfin[1], Emma Hasina Massasa[1], Arad Lang[1], Shai Levy[1], Lotte T.J. Kortstee[3], Betty Shamaev[1], Shaked Dror[1], Rachel Lifer[1], Reut Shechter[1], Yaron Kauffmann[1], Rotem Strassberg[1,5], Iryna Polishchuk[1], Andrew Barnabas Wong[4], Boaz Pokroy[1], Ivano E. Castelli[3] and Yehonadav Bekenstein*[1,2,5]

Affiliations:

[1]Department of Materials Science and Engineering, Technion – Israel Institute of Technology, 32000 Haifa, Israel.

[2]The Nancy and Stephen Grand Technion Energy Program, Technion – Israel Institute of Technology, 32000 Haifa, Israel.

[3]Department of Energy Conversion and Storage (DTU Energy), Technical University of Denmark, Anker Engelunds Vej 301, 2800 Kongens Lyngby, Denmark.

[4]Department of Materials Science and Engineering, College of Design and Engineering, National University of Singapore, 21 Lower Kent Ridge Rd 119077, Singapore.

[5]The Solid-state institute, Technion – Israel Institute of Technology, 32000 Haifa, Israel.

*Corresponding author. Email: bekenstein@technion.ac.il

Methods

Materials

Antimony (III) acetate (99.9%, Aldrich), benzoyl chloride (99.9%, Alfa Aesar), bismuth (III) acetate (99.9%, Aldrich), cesium carbonate (99.9%, Aldrich), hexane (A.R. Aldrich or 99.9%, Fischer Scientific), indium (III) acetate (99.9%, Aldrich), octadecene (90%, Aldrich), oleic acid (90%, Aldrich), oleylamine (70%, Aldrich), silver acetate (99.9%, Aldrich), sodium acetate (99.9%, Aldrich). All chemicals were used as purchased with no further purifications.

Synthesis of 0.5M Cs-oleate precursor

The Cs-oleate solution was prepared following the approach of F. Locardi et al.[1] 1.63gr (5mmol) of Cs_2CO_3, 20ml (63.37mmol) of oleic acid, and a stirring bar were inserted into a 50ml three-necked round bottom flask. The flask was plugged into a Schenck line and degassed under vacuum and 100°C for 30 minutes or until there were no bubbles. Then, the temperature was raised to 150°C under nitrogen and stirred for 3 hours. The product was a clear yellow solution.

Synthesis of 0.25M Sb-oleate, 0.25M In-oleate and 0.5M Na-oleate precursors

0.7472gr (2.5mmol) of Sb(ac)$_3$ or 0.7299gr (2.5mmol) of In(ac)$_3$ or 0.4102gr (5mmol) of Na(ac), 10ml (31.7mmol) of oleic acid and a stirring bar were inserted into 20ml glass vile. The reaction was stirred for 45 minutes at 90°C in an open-air environment. The Sb-oleate and Na-oleate products were slightly yellow, clear solutions. The In-

oleate product was a clear solution while warm and a solid white paste while cold (room temperature).

Synthesis of $Cs_2Ag_{1-y}Na_yIn_{1-x}Bi_xCl_6$ NC's

$Cs_2Ag_{1-y}Na_yIn_{1-x}Bi_xCl_6$ nanocrystals were synthesized using the procedures developed by F. Locardi et al.[1] with several modifications. 0.24mmol of Ag(ac) and Na(ac), 0.25mmol of In(ac)$_3$ and Bi(ac)$_3$, 1ml of 0.5M Cs-oleate solution (0.5mmol), 0.5ml oleylamine (1.52mmol), 4.5ml of ODE and a stirring bar were inserted into 20ml glass vile. The mixture was stirred for 5 minutes at 100°C in an open-air environment. Then, 200µl of Bz-Cl (1.72mmol) were swiftly injected. The reaction was stirred for another 5 seconds and then cooled in a cold water bath. The solution was then centrifuged, first at 7000rpm for 10 minutes, and the precipitation was redispersed in 5ml hexane and then centrifuged at 3500rpm for 5 minutes. The solution was transferred to a new tube and centrifuged again at 7000rpm for 10 minutes and separated from the residue.

Synthesis of $Cs_2Ag_{1-y}Na_yIn_{1-x}Sb_xCl_6$ NC's

0.24mmol of Ag(ac) and 0.5M Na-oleate solution, 0.25mmol of 0.25M In-oleate solution and Sb-oleate solution, 1ml of 0.5M Cs-oleate solution (0.5mmol), 0.5ml oleylamine (1.52mmol), 4.5ml of ODE and a stirring bar were inserted into 20ml glass vile. The mixture was stirred for 5 minutes at 100°C in an open-air environment. Then, 200µl of Bz-Cl (1.72mmol) were swiftly injected. The reaction was stirred for another 5 seconds and then cooled in a cold water bath. The solution was then centrifuged, first at 7000rpm for 10 minutes, and the precipitation was redispersed in 5ml hexane and then centrifuged at 3500rpm for 5 minutes. The solution was transferred to a new tube, centrifuged at 7000rpm for 10 minutes, and separated from the residue.

Optical characterizations

The absorption, emission, and PLE characterizations were performed using a Gen5 Synergy H1 hybrid multi-mode reader spectrophotometer with 99 wells plates. All the measurements were performed with the products inside the hexane emulsion solution and with a reference blank well of clean hexane. All the measurements were performed using a step size of 1nm wavelength and intensity gain of 50 or 100, depending on the specific product and the solution concentration.

Lifetime and photoluminescence quantum yield (PLQY) characterizations were performed using the Edinburgh FLS1000 photoluminescence spectrometer. All the samples were loaded into a quartz cuvette. The lifetime measurements were performed with multi-channel scaling (MCS) mode and conducted using a variable pulse laser (VPL). The PLQY measurements were performed with an integrating sphere holder inside the spectrometer.

Temperature-dependent photoluminescence was performed using the Edinburgh FLS1000 photoluminescence spectrometer coupled to Nikon Eclipse UPRIGHT Ni-U architecture light microscope with THMS350V temperature controlled vacuum system stage with LNP95. The NC's solution in hexane was centrifuged at 12000rpm for 10 minutes, and the residue was drop-cast onto p-type silicon wafer slice ($10x10mm^2$). The measurements were taken at the range from 80K to 300K with steps of 20K.

X-ray diffraction (XRD) characterizations

The NC's solution in hexane was centrifuged at 12000rpm for 10 minutes, and the residue was drop-cast onto a rectangular micro slide glass substrate (76mmx26mm). Measurements were taken using a Rigaku Smart-Lab 9kW high-resolution X-ray diffractometer, equipped with a rotating anode X-ray source. We used a 1.54Å (Cu Kα) wavelength and a 2θ range of 10º-90º.

High resolution powder X-ray diffraction (HRPXRD)

The NC's solution in hexane was centrifuged at 12000rpm for 10 minutes, and the residue was smeared onto a capillary. The samples were measured by the ID22 beamline of the European Synchrotron Radiation Facility (ESRF) in Grenoble, France, at room temperature, using a wavelength of 0.35423 Å.

Transmission electron microscopy (TEM) characterizations

A drop of dilute NC's solution in hexane was cast onto a TEM grid – carbon film only on 300 mesh copper, and observed in TEM mode using a FEI/Thermo-Fisher Tecnai G^2 T20 with LaB_6 electron source operated at an accelerating voltage of 200KeV.

High-angle annular dark-field scanning transmission electron microscopy (HAADF-STEM)

A TEM grid was prepared the same as for the TEM characterization and observed in HAADF-STEM mode using a FEI/Thermo-Fisher double corrected 60-300 Titan Themis FEG-S/TEM operated at an accelerating voltage of 200KeV.

Scanning electron microscopy (SEM) and energy dispersive X-ray spectroscopy (EDS)

The NC's solution in hexane was centrifuged at 12000rpm for 10 minutes, and the residue was drop-cast onto p-type silicon wafer slice ($10x10mm^2$). SEM micrographs were taken using HR-SEM microscope model Zeiss Ultra-Plus. Samples were placed at a working distance of 7mm and measured using acceleration voltage of 15 kV.

Density Functional Theory (DFT) calculations

Crystal structure investigation for $Cs_2Ag_{0.4}Na_{0.6}In_{1-x}Bi_xCl_6$, and $Cs_2NaIn_{1-x}Sb_xCl_6$ bulk double perovskites were performed using DFT calculations using the GPAW code[2,3].

All relaxations have been performed in the Generalized Gradient Approximation (GGA) framework, within the description of the PBEsol[4] exchange-correlation functional, using the Plane Wave mode (cutoff of 700 eV) and a Γ-centered k-point Monkhorst-Pack mesh of 4 k-point/Å. All structures have been fully relaxed until the residual forces on all atoms were below 0.01 eV/Å. The distribution of cations in a $2\sqrt{2}x2\sqrt{2}x2$ supercell were generated to maximize the symmetries between the different cations. For reproducibility and reusability of the results, all input and output files have been collected in a repository freely available on DTU Data.[5] Electronic properties were calculated starting from the relaxed structures using the GLLB-SC functional.[6] By including the calculation of the derivative discontinuity, the GLLB-SC method calculates band gaps with a similar accuracy of the GW and HSE06 at the computational cost of a GGA calculation.[7,8] Spin-orbit coupling (SOC) corrections were also included. The Atomistic Simulation Environment (ASE) package[9] has been used to create and operate with the structures.
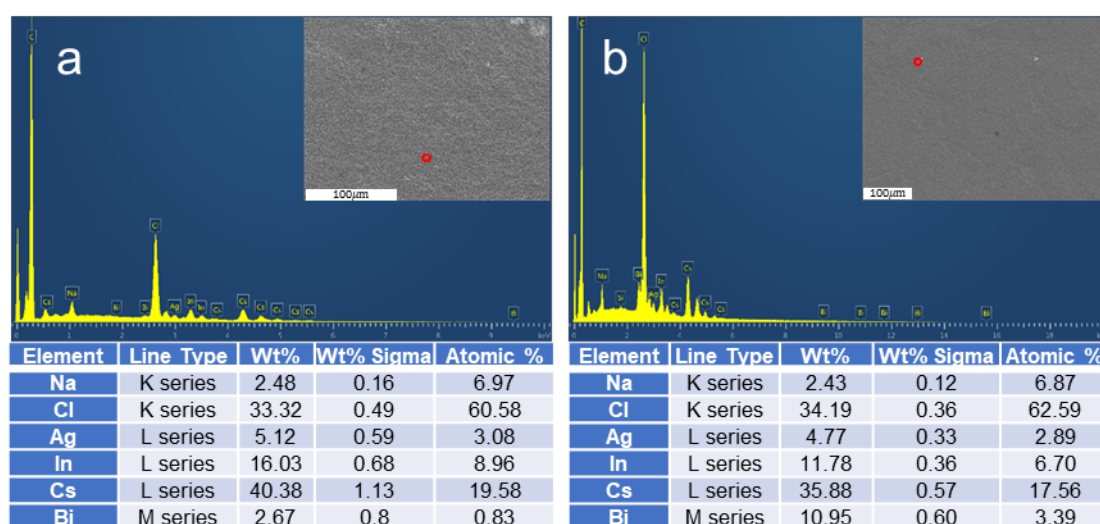
Results

Element	Line Type	Wt%	Wt% Sigma	Atomic %
Na	K series	2.48	0.16	6.97
Cl	K series	33.32	0.49	60.58
Ag	L series	5.12	0.59	3.08
In	L series	16.03	0.68	8.96
Cs	L series	40.38	1.13	19.58
Bi	M series	2.67	0.8	0.83

Element	Line Type	Wt%	Wt% Sigma	Atomic %
Na	K series	2.43	0.12	6.87
Cl	K series	34.19	0.36	62.59
Ag	L series	4.77	0.33	2.89
In	L series	11.78	0.36	6.70
Cs	L series	35.88	0.57	17.56
Bi	M series	10.95	0.60	3.39

Figure S1: SEM-EDS of $Cs_2Ag_{0.4}Na_{0.6}In_{1-x}Bi_xCl_6$ NC's with (a) x=0.05 and (b) x=0.25. The ratios in the chemical formula are referring to the loading ratios in the reaction mixture. The samples were placed at a working distance of 7mm and measured using acceleration voltage of 15 kV. The atomic percentage shows sub-stochiometric ratios, close to the loading ratios, with some deviations.
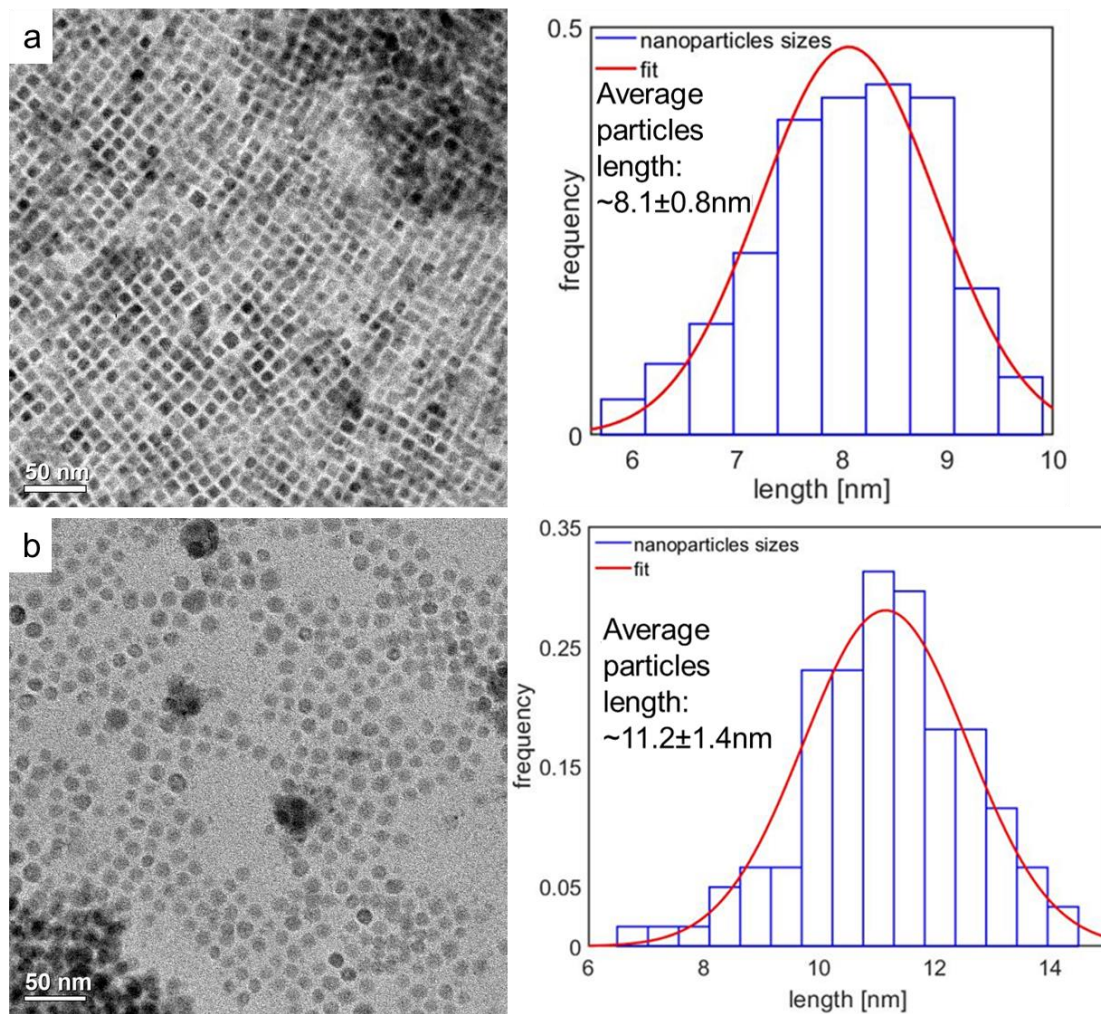
Figure S2: TEM micrograph and size distribution of (a) Bi-doped $Cs_2Ag_{0.5}Na_{0.5}InCl_6$ NC's and (b) Sb-doped $Cs_2NaInCl_6$ NC's.
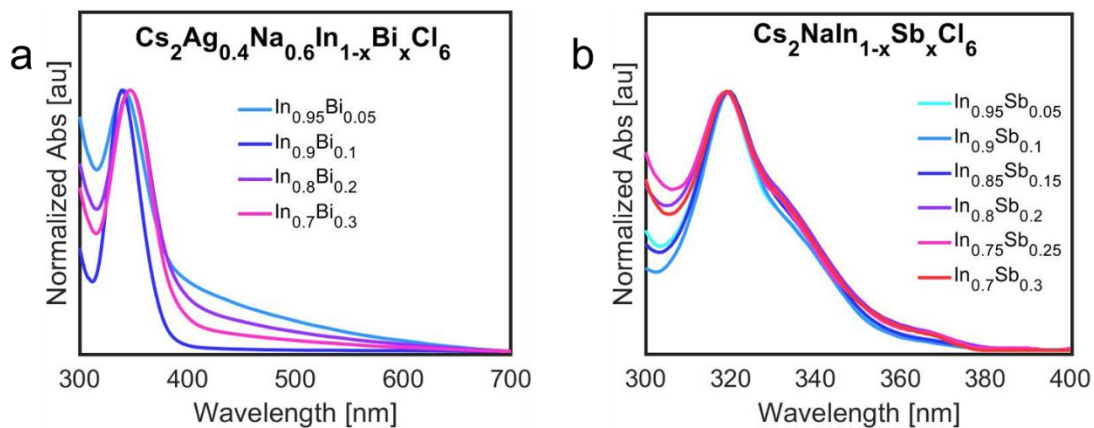
Figure S3: Normalized absorption (Abs) of (a) $Cs_2Ag_{0.4}Na_{0.6}In_{1-x}Bi_xCl_6$ (x=0.05, 0.1, 0.2, 0.3) and (b) $Cs_2NaIn_{1-x}Sb_xCl_6$ (x=0.05, 0.1, 0.15, 0.2, 0.25, 0.3).
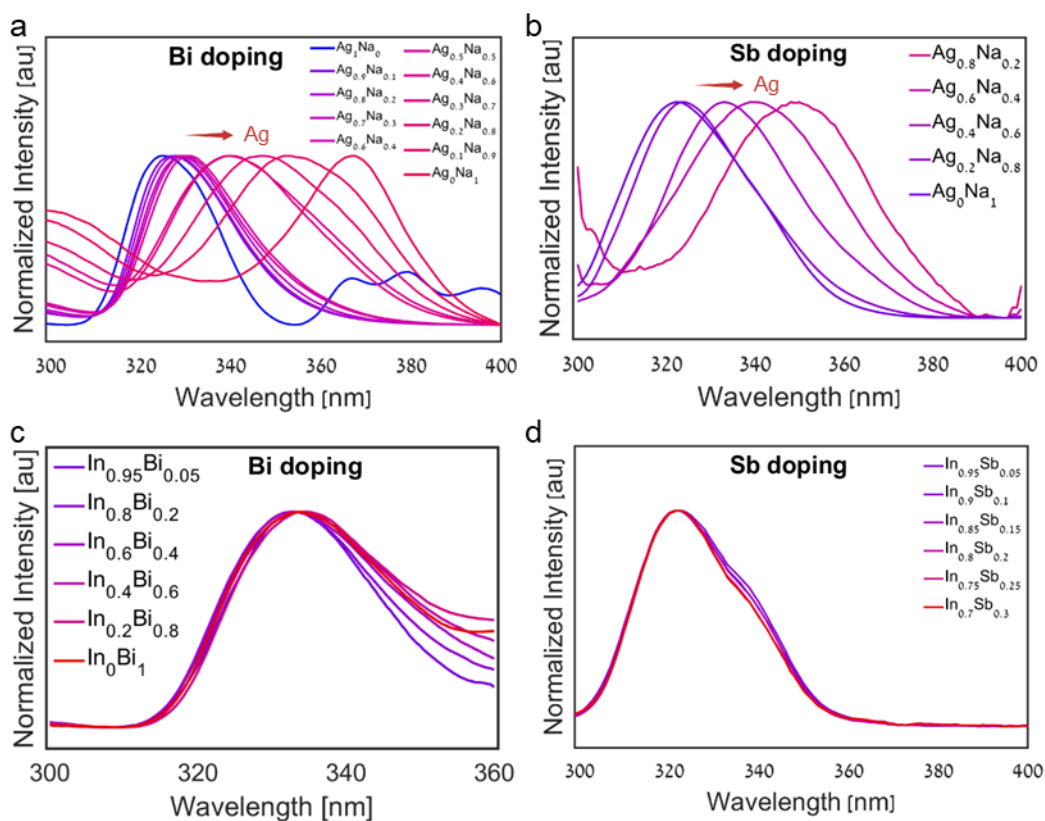
Figure S4: Normalized photoluminescence excitation (PLE) of (a) $Cs_2Ag_{1-y}Na_yIn_{0.9}Bi_{0.1}Cl_6$ (y=0, 0.1, 0.2, 0.3, 0.4, 0.5, 0.6, 0.7, 0.8, 0.9, 1), (b) $Cs_2Ag_{1-y}Na_yIn_{0.9}Sb_{0.1}Cl_6$ (y=0.2, 0.4, 0.6, 0.8, 1), (c) $Cs_2Ag_{0.4}Na_{0.6}In_{1-x}Bi_xCl_6$ (x=0.05, 0.2, 0.4, 0.6, 0.8, 1), and (d) $Cs_2NaIn_{1-x}Sb_xCl_6$ (x=0.05, 0.1, 0.15, 0.2, 0.25, 0.3). The emission wavelength for (a) is 620nm, for (b) between 450nm to 580nm at the emission peaks, for (c) between 610nm to 680nm at the emission peaks, and for (d) is 450nm.
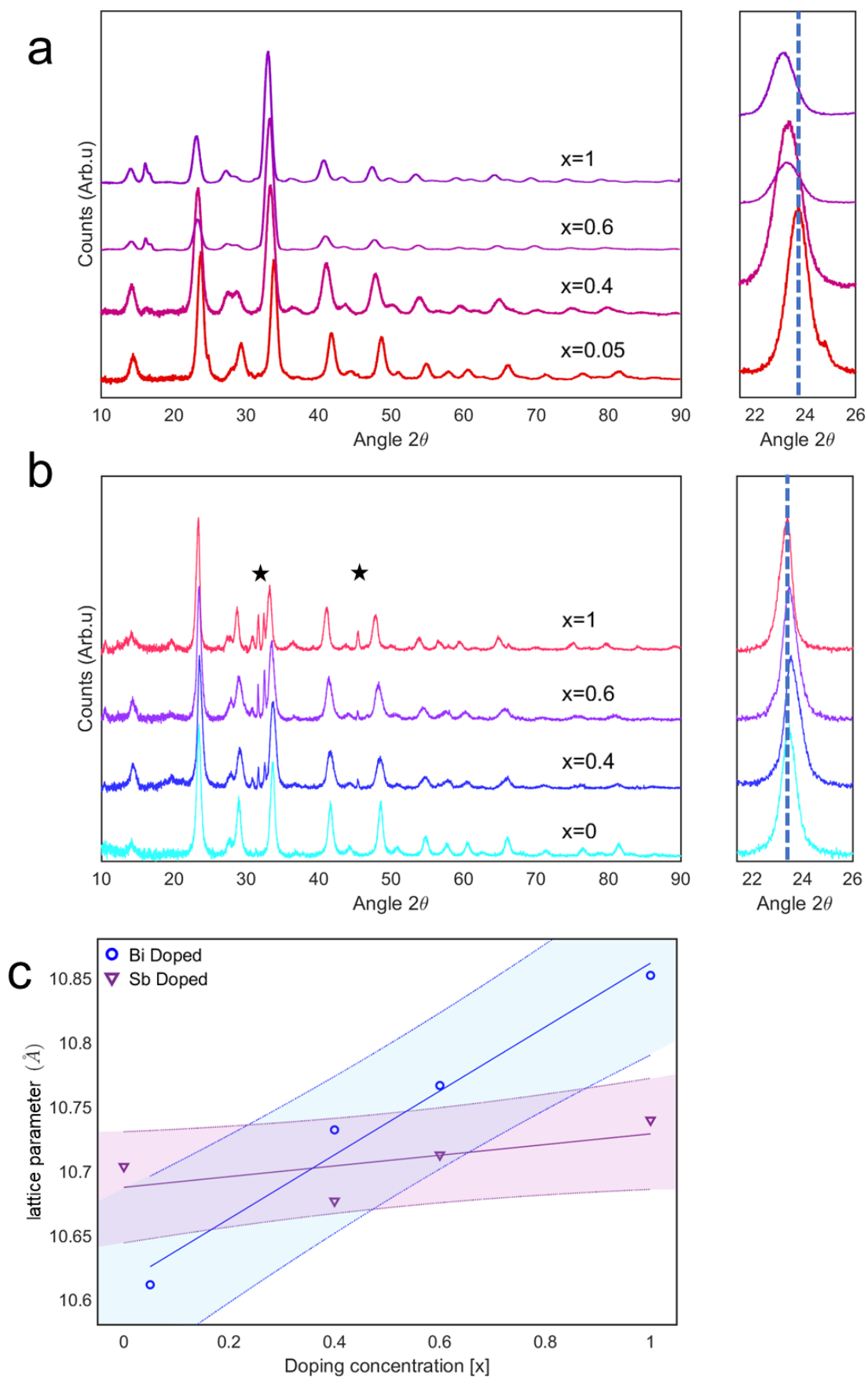
Figure S5: X-ray diffraction (XRD) patterns of (a) $Cs_2Ag_{0.4}Na_{0.6}In_{1-x}Bi_xCl_6$ (x=0, 0.4, 0.6, 1) nanoparticles and (b) $Cs_2NaIn_{1-x}Sb_xCl_6$ (x=0, 0.4, 0.6, 1) nanoparticles, and (c) the lattice

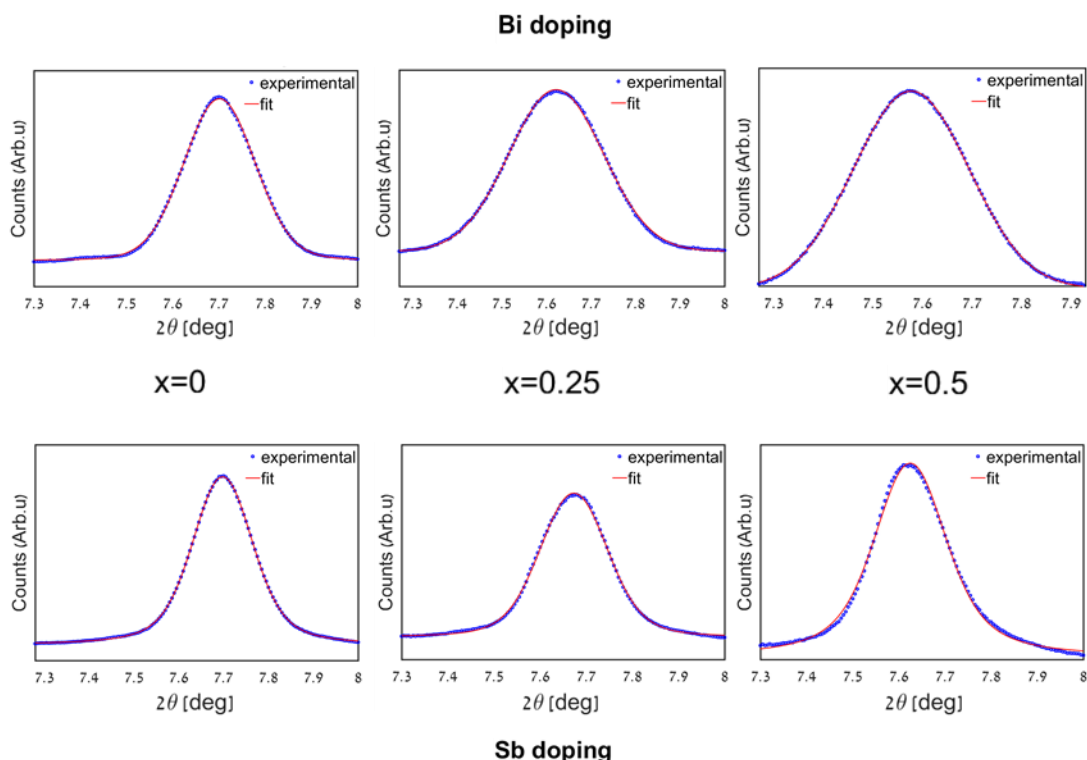parameters, calculated from the XRD patterns. NaCl peaks marked with black stars (ICDD no. 04-020-4596).

Bi doping

x=0   x=0.25   x=0.5

Sb doping

Figure S6: Synchrotron High resolution powder X-ray diffraction (HRPXRD) (λ=0.35423Å wavelength) (400) peak of $Cs_2Ag_{0.4}Na_{0.6}In_{1-x}Bi_xCl_6$ NC's with (a) x=0, (b) x=0.25, and (c) x=0.5; and $Cs_2NaIn_{1-x}Sb_xCl_6$ NC's with (d) x=0, (e) x=0.25, and (f) x=0.5. The peaks are fitted to a Voigt function to extract the averaged micro-strain fluctuations, using the Gaussian part: $= \frac{W_G}{4\sqrt{2\ln 2}\tan\theta_B}$, where W_G is the Gaussian width, and θ_B is the Bragg's angle[10]. The fitting parameters of the Voigt function are listed in the table below:

| sample	height		position		integral		Gaussian FWHM		Lorenzian FWHM		Peak FWHM		Statistics	
	y_0		x_c		A		W_G		W_L		FWHM			
		Stdev		Stdev		Stdev		Stdev		Stdev		Stdev	Red. χ^2	Adj. R^2
0%Sb	586	5	7.69784	6E-5	1249	5	0.1222	8E-4	0.064	0.001	0.1602	2E-4	375.2537	0.9999
25%Sb	417	8	7.6731	2E-4	553	8	0.149	0.003	0.045	0.005	0.1745	6E-4	616.2788	0.99922
50%Sb	542	16	7.6247	4E-4	674	17	0.123	0.006	0.104	0.008	0.188	0.001	1850.992	0.99753
0%Bi	726	10	7.7014	1E-4	908	10	0.171	0.002	0.019	0.004	0.1818	4E-4	1002.693	0.99957
25%Bi	654	4	7.6220	2E-4	790	3	0.2487	6E-4	3E-15	8E-4	0.2487	6E-4	494.9807	0.99956
50%Bi	740	3	7.5774	1E-4	854	2	0.2747	5E-4	1E-18	0	0.2747	5E-4	187.2622	0.99982
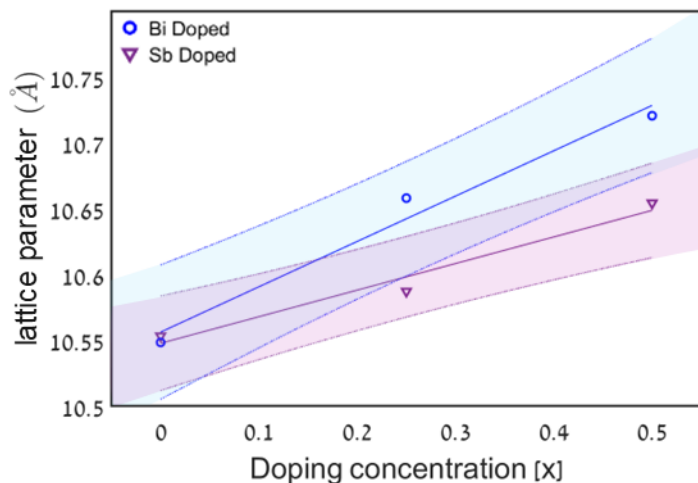
Figure S7: The lattice parameters, calculated using the (400) diffraction peaks from the synchrotron High resolution powder X-ray diffraction (HRPXRD) (λ=0.35423Å wavelength) and the positions of the Voigt function fit in the table above (figure S6).
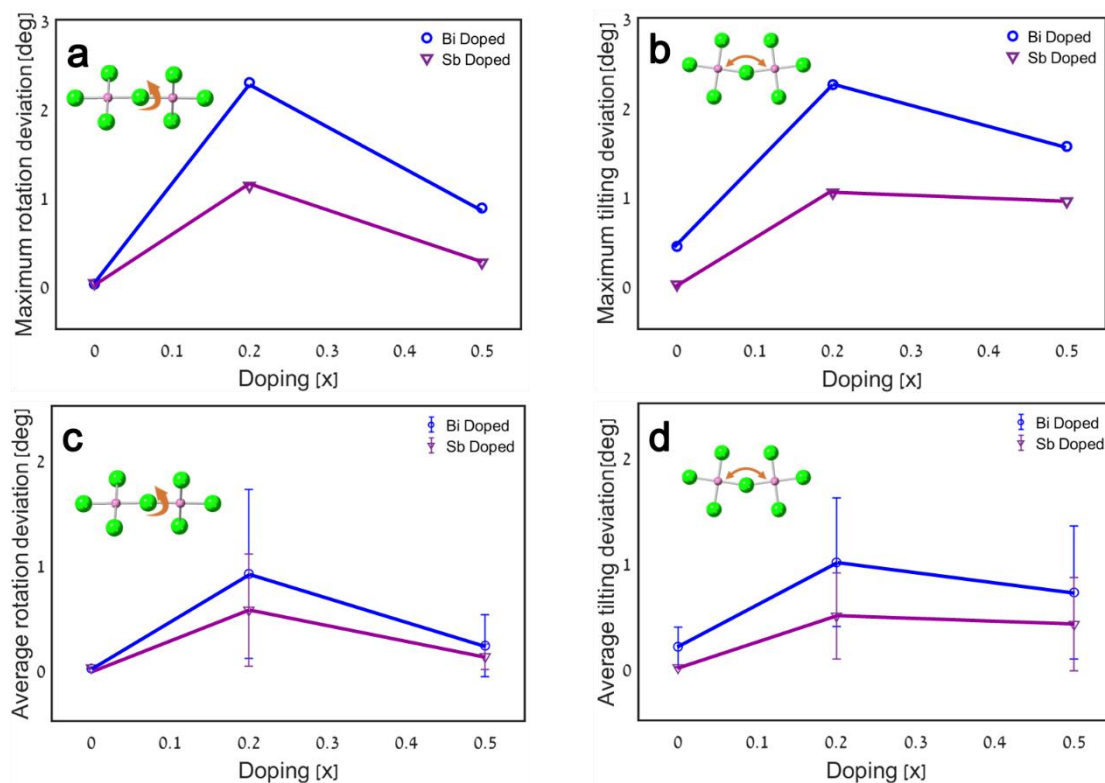

Figure S8: (a) Maximum rotation deviation, (b) maximum tilting deviation, (c) average rotation deviation, and (d) average tilting deviation of $Cs_2NaIn_{1-x}Sb_xCl_6$ and $Cs_2Ag_{0.4}Na_{0.6}In_{1-x}Bi_xCl_6$ (x=0, 0.25, 0.5). The rotation/tilting angles were extracted based on the DFT modeling, and the deviations were calculated from the difference from the original non rotated/tilted angles.
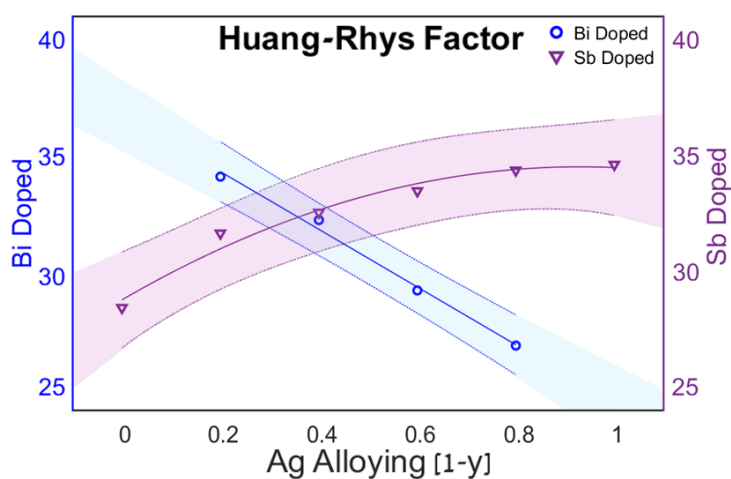
Figure S9: Huang-Rhys factor of $Cs_2Ag_{1-y}Na_yIn_{0.9}Bi_{0.1}Cl_6$ (y=0.2, 0.4, 0.6, 0.8), and $Cs_2Ag_{1-y}Na_yIn_{0.9}Sb_{0.1}Cl_6$ (y=0, 0.2, 0.4, 0.6, 0.8, 1).
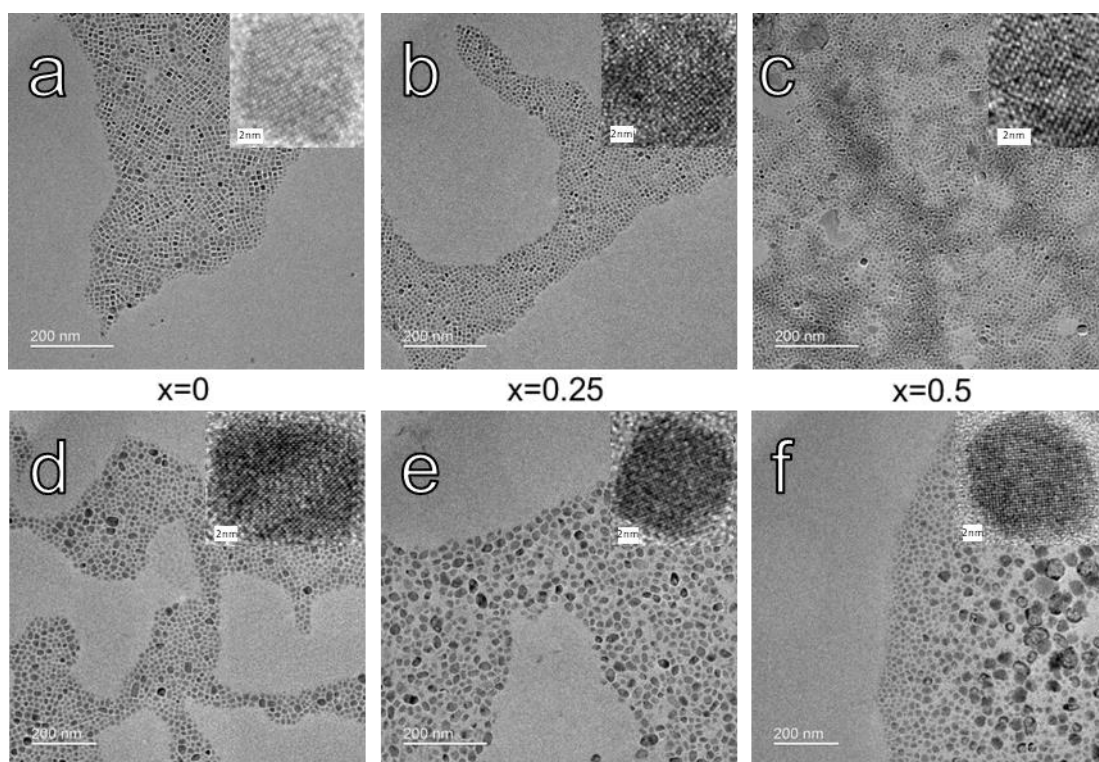
Figure S10: TEM and HRTEM micrographs of $Cs_2Ag_{0.4}Na_{0.6}In_{1-x}Bi_xCl_6$ NC's with (a) x=0, (b) x=0.25, and (c) x=0.5; and $Cs_2NaIn_{1-x}Sb_xCl_6$ NC's with (d) x=0, (e) x=0.25, and (f) x=0.5. The $Cs_2Ag_{0.4}Na_{0.6}In_{1-x}Bi_xCl_6$ micrographs shows relatively homogenous cubic nanoparticles, while the $Cs_2NaIn_{1-x}Sb_xCl_6$ micrographs show a non-homogenous nanoparticle. The non-homogeneity increased with the doping concentration of Sb. For x=0.5 with Sb doping, there is an apparent beam damage of the nanoparticles.
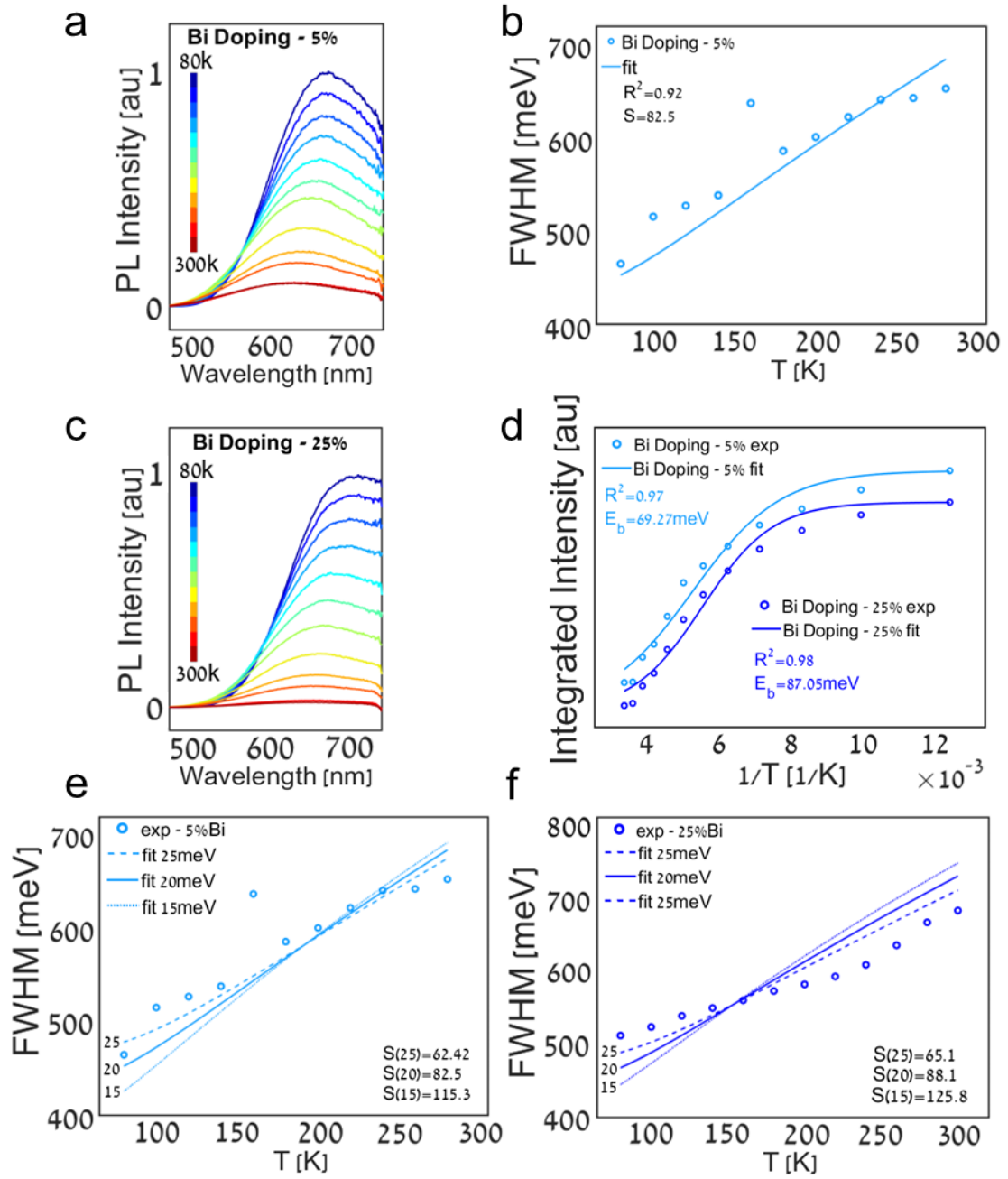
Figure S11: (a) Temperature-dependent photoluminescence of $Cs_2Ag_{0.4}Na_{0.6}In_{0.95}Bi_{0.05}Cl_6$ and (b) temperature-dependent FWHM with Calculated Huang-Rhys factor. (c) Temperature-dependent photoluminescence of $Cs_2Ag_{0.4}Na_{0.6}In_{0.75}Bi_{0.25}Cl_6$. (d) Temperature-dependent integrated intensity of (a) and (c) with calculated binding energy (E_b=69.27meV and 87.05meV, respectively). Temperature-dependent FWHM with Calculated Huang-Rhys factor with $\hbar\omega$=15,20,25meV for (e) 5% Bi doping and (f) 25% Bi doping.

Calculation of Huang-Rhys factor and E_b:

Fitting the dependence of the FWHM on the temperature we extracted the Huang-Rhys factor S using:

$$FWHM = 2.36\sqrt{S}\hbar\omega_{phonons}\sqrt{\coth\left(\frac{\hbar\omega_{phonons}}{2K_BT}\right)},$$

where $\hbar\omega$ is the phonon frequency, K_B is the Boltzmann constant, and T is the temperature. We calculated a Huang-Rhys factor of 82.5 for $Cs_2Ag_{0.4}Na_{0.6}In_{0.95}Bi_{0.05}Cl_6$ with $\hbar\omega$=20meV. This value is about two times larger than the Huang-Rhys factor calculated using the Stokes shift (as discussed earlier). We note that the temperature-dependent FWHM should produce a more accurate value. Still, due to experimental limitations, not all of the emission range could be measured, and the FWHM was evaluated using only half width at the half maximum. We used a gaussian fit to extract the FWHM from the PL emission data, to ensure uniform analysis and better fit of the both 5% and 25% of Bi doping.

Fitting the dependence of the integrated intensity on the temperature, we extracted the binding energy E_b using:

$$I = I_0/\left(1 + e^{-E_b/K_bT}\right),$$

Where I is the intensity, I_0 is the integrated intensity in 0K (here, it is the highest integrated intensity), K_B is the Boltzmann constant, and T is the temperature[11,12]. The binding energy of the 25% Bi sample is higher than the binding energy of the 5% Bi sample by ~18meV. As mentioned above, due to experimental limitations, not all of the emission range could be measured, and the integrated intensity was calculated only on the partial range. This might lead to inaccurate results, especially for the 25% Bi sample, where the emission peak is red-shifted.

References

(1)   Locardi, F.; Cirignano, M.; Baranov, D.; Dang, Z.; Prato, M.; Drago, F.; Ferretti, M.; Pinchetti, V.; Fanciulli, M.; Brovelli, S.; De Trizio, L.; Manna, L. Colloidal Synthesis of Double Perovskite $Cs_2AgInCl_6$ and Mn-Doped $Cs_2AgInCl_6$ Nanocrystals. *J. Am. Chem. Soc.* **2018**, *140* (40), 12989–12995.

(2)   Mortensen, J. J.; Hansen, L. B.; Jacobsen, K. W. Real-Space Grid Implementation of the Projector Augmented Wave Method. *Phys. Rev. B - Condens. Matter Mater. Phys.* **2005**, *71* (3).

(3)   Enkovaara, J.; Rostgaard, C.; Mortensen, J. J.; Chen, J.; Dułak, M.; Ferrighi, L.; Gavnholt, J.; Glinsvad, C.; Haikola, V.; Hansen, H. A.; Kristoffersen, H. H.; Kuisma, M.; Larsen, A. H.; Lehtovaara, L.; Ljungberg, M.; Lopez-Acevedo, O.; Moses, P. G.; Ojanen, J.; Olsen, T.; Petzold, V.; Romero, N. A.; Stausholm-Møller, J.; Strange, M.; Tritsaris, G. A.; Vanin, M.; Walter, M.; Hammer, B.; Häkkinen, H.; Madsen, G. K. H.; Nieminen, R. M.; Nørskov, J. K.; Puska, M.; Rantala, T. T.; Schiøtz, J.; Thygesen, K. S.; Jacobsen, K. W. Electronic structure calculations with GPAW: a real-space implementation of the projector augmented-wave method. *J. Phys. Condens. Matter.*

2010, 22 (24pp), 253202.

(4)   Perdew, J. P.; Ruzsinszky, A.; Csonka, G. I.; Vydrov, O. A.; Scuseria, G. E.; Constantin, L. A.; Zhou, X.; Burke, K. Restoring the Density-Gradient Expansion for Exchange in Solids and Surfaces. *Phys. Rev. Lett*. **2008**, 100, 136406.

(5)   Dataset for: How does local strain affect Stokes shifts in halide double perovskite nanocrystals? *DTU data*. **2023**, 10.11583/DTU.24099795.

(6)   Kuisma, M.; Ojanen, J.; Enkovaara, J.; Rantala, T. T. Kohn-Sham Potential with Discontinuity for Band Gap Materials. *Phys. Rev. B - Condens. Matter Mater. Phys.* **2010**, *82* (11), 115106.

(7)   Castelli, I. E.; Olsen, T.; Datta, S.; Landis, D. D.; Dahl, S.; Thygesen, K. S.; Jacobsen, K. W. Computational Screening of Perovskite Metal Oxides for Optimal Solar Light Capture. *Energy Environ. Sci*. **2012** ,5 ,5814-5819.

(8)   Castelli, I. E.; Hüser, F.; Pandey, M.; Li, H.; Thygesen, K. S.; Seger, B.; Jain, A.; Persson, K. A.; Ceder, G.; Jacobsen, K. W. New Light-Harvesting Materials Using Accurate and Efficient Bandgap Calculations. *Adv. Energy Mater.* **2015**, *5* (2), 1400915.

(9)   Larsen, A. H.; Mortensen, J. J.; Blomqvist, J.; Castelli, I. E.; Christensen, R.; Dułak, M.; Friis, J.; Groves, M. N.; Hammer, B.; Hargus, C.; Hermes, E. D.; Jennings, P. C.; Jensen, P. B.; Kermode, J.; Kitchin, J. R.; Kolsbjerg, E. L.; Kubal, J.; Kaasbjerg, K.; Lysgaard, S.; Maronsson, J. B.; Maxson, T.; Olsen, T.; Pastewka, L.; Peterson, A.; Rostgaard, C.; SchiØtz, J.; Schütt, O.; Strange, M.; Thygesen, K. S.; Vegge, T.; Vilhelmsen, L.; Walter, M.; Zeng, Z.; Jacobsen, K. W. The Atomic Simulation Environment—a Python Library for Working with Atoms. *J. Phys. Condens. Matter* **2017**, *29* (27), 273002.

(10)   Pokroy, B.; Fitch, A.; Zolotoyabko, E. The Microstructure of Biogenic Calcite: A View by High-Resolution Synchrotron Powder Diffraction. *Adv. Mater.* **2006**, *18* (18), 2363–2368.

(11)   Wolf, C.; Lee, T.-W. Exciton and Lattice Dynamics in Low-Temperature Processable $CsPbBr_3$ Thin-Films. *Materials Today Energy*. **2017**, 7, 199-207.

(12)   Zeng, R.; Zhang, L.; Xue, Y.; Ke, B.; Zhao, Z.; Huang, D.; Wei, Q.; Zhou, W.; Zou, B. Highly Efficient Blue Emission from Self-Trapped Excitons in Stable Sb^{3+}-Doped $Cs_2NaInCl_6$ Double Perovskites. *J. Phys. Chem. Lett.* **2020**, 11, 6, 2053–2061.